Tricritical behavior of the two-dimensional intrinsically ferromagnetic semiconductor $CrGeTe_3$

G. T. Lin,[1,2] H. L. Zhuang,[3] X. Luo,[1,*] B. J. Liu,[2,4] F. C. Chen,[1,2] J. Yan,[1,2] Y. Sun,[2,4] J. Zhou,[5] W. J. Lu,[1] P. Tong,[1] Z. G. Sheng,[4,6] Z. Qu,[4] W. H. Song,[1] X. B. Zhu,[1] and Y. P. Sun[1,4,6,†]

[1]*Key Laboratory of Materials Physics, Institute of Solid State Physics, Chinese Academy of Sciences, Hefei 230031, China*

[2]*University of Science and Technology of China, Hefei 230026, China*

[3]*Department of Mechanical and Aerospace Engineering, Princeton University, Princeton, New Jersey 08544, USA*

[4]*High Magnetic Field Laboratory, Chinese Academy of Sciences, Hefei 230031, China*

[5]*MIIT Key Laboratory of Critical Materials Technology for New Energy Conversion and Storage, School of Chemistry and Chemical Engineering, Harbin Institute of Technology, Harbin 150001, China*

[6]*Collaborative Innovation Center of Advanced Microstructures, Nanjing University, Nanjing 210093, China*

(Received 6 April 2017; published 30 June 2017)

$CrGeTe_3$ recently emerges as a new two-dimensional (2D) ferromagnetic semiconductor that is promising for spintronic device applications. Unlike $CrSiTe_3$ whose magnetism can be understood using the 2D-Ising model, $CrGeTe_3$ exhibits a smaller van der Waals gap and larger cleavage energy, which could lead to a transition of magnetic mechanism from 2D to 3D. To confirm this speculation, we investigate the critical behavior of $CrGeTe_3$ around the second-order paramagnetic-ferromagnetic phase transition. We obtain the critical exponents estimated by several common experimental techniques including the modified Arrott plot, Kouvel-Fisher method, and critical isotherm analysis, which show that the magnetism of $CrGeTe_3$ follows the tricritical mean-field model with the critical exponents β, γ, and δ of 0.240 ± 0.006, 1.000 ± 0.005, and 5.070 ± 0.006, respectively, at the Curie temperature of 67.9 K. We therefore suggest that the magnetic phase transition from 2D to 3D for $CrGeTe_3$ should locate near a tricritical point. Our experiment provides a direct demonstration of the applicability of the tricritical mean-field model to a 2D ferromagnetic semiconductor.

DOI: 10.1103/PhysRevB.95.245212

I. INTRODUCTION

Since the successful exfoliation of single-layer graphene, two-dimensional (2D) materials have been attracting significant interest due to their highly tunable physical properties and immense potential in scalable device applications [1–5]. However, pristine graphene exhibits no band gap and its inherent inversion symmetry suppresses the spin-orbit coupling (SOC) [6–11]. The weak SOC and zero band gap eliminate graphene as a potential candidate for being applied to spintronic devices, which require one to search for alternative 2D materials that extend beyond graphene to other layered materials with van der Waals gaps [7–11]. For example, in single-layer MoS_2, the large SOC leads to a unique spin-valley coupling which may be useful for spintronic applications [12–16]; whereas, spintronic devices using 2D materials are still in their infancy [17–20], which is due to the lack of long-range ferromagnetic order that is crucial for macroscopic magnetic effects [21,22]. The emergence of ferromagnetism in 2D materials in combination with their rich electrical and optical properties could open up ample opportunities for 2D magnetic, magnetoelectric, and magneto-optic applications [18,19,23].

Recently, chromium tellurides $CrXTe_3$ (X = Si, Ge, and Sn) with the centrosymmetric structure have attracted significant attention because they belong to a rare category of ferromagnetic semiconductors possessing a 2D layered structure [7,23–35]. Extensive theoretical and experimental efforts have been extended toward understanding the properties of these 2D magnets. On the theoretical side, recent studies on $CrXTe_3$ have been focusing on their electronic structure and magnetic properties, particularly predictions of the single-layer properties [24,28–33]. On the experimental side, $CrSiTe_3$ and $CrGeTe_3$ have been prepared and characterized [7,23,25–27,34,35]. Comparing with $CrSiTe_3$, showing characteristics of a 2D-Ising behavior [7,34,35], the smaller van der Waals gap and the larger in-plane nearest-neighbor Cr-Cr distance in $CrGeTe_3$ enhance the Curie temperature from 32 K for the $CrSiTe_3$ to 61 K for the $CrGeTe_3$ [7,25,28,31]. In addition, theoretical investigations have suggested that the single-layer $CrGeTe_3$ presents characteristics of 2D-Ising behavior similar to $CrSiTe_3$ [31,33]. By contrast, in a scanning magneto-optic Kerr microscopy experiment, single-layer $CrGeTe_3$ represents a close-to-ideal 2D Heisenberg ferromagnetic system using the rigorous renormalized spin wave theory analysis and calculations [23]. It is known that, with the increase of the X atom radius, $CrXTe_3$ presents the smaller van der Waals gap and the larger cleavage energy [7,25,28,31]. We suppose that the $CrXTe_3$ system may undergo a three-dimensional (3D) magnetic phase transition from 2D with the increase of the X atom radius. Therefore, a method to rapidly characterize the critical behavior of single-crystalline $CrGeTe_3$ is crucial. For this purpose, we present a detailed investigation of the critical phenomena of $CrGeTe_3$ using the initial isothermal $M(H)$ curves around the Curie temperature T_C. We find that the critical exponents of $CrGeTe_3$ satisfy the universality class of the tricritical mean-field theory. This indicates that the magnetic phase transition of $CrGeTe_3$ should be close to a tricritical point from 2D to 3D.

II. METHODS

Samples of single-crystalline $CrGeTe_3$ were prepared by the self-flux technique [26]. The x-ray diffraction (XRD)

*xluo@issp.ac.cn
†ypsun@issp.ac.cn

data indicated that the powders are single phase with the rhombohedral structure (see the Supplemental Material [36]). We measured the heat capacity using the Quantum Design physical properties measurement system (PPMS-9T) and characterized the magnetic properties by the magnetic property measurement system (MPMS-XL5). Density functional theory (DFT) calculations were performed using the Vienna *ab-initio* simulation package [37]. We used the local density approximation [38,39] to treat the electron-electron exchange-correlation interactions. The electron-ion interactions are described by the potentials based on the projector augmented wave method [40,41].

III. RESULTS

Figures 1(a) and 1(b) show the temperature-dependent inverse susceptibility $1/\chi(T)$ of $CrGeTe_3$ under field cooled cooling with applied magnetic field $H = 100$ Oe, parallel to the ab plane and c axis, respectively. We observe a paramagnetic-ferromagnetic (PM-FM) transition that occurs at a critical temperature of 67.3 K, as determined by the derivative of the susceptibility. This temperature is consistent with the values of 61 or 70 K reported previously [25–27]. For a FM system, the $1/\chi(T)$ above T_C can be described by the Curie-Weiss law resulting from the mean-field theory [42]. The red curves showing the Curie-Weiss law are obeyed only at high temperatures. A close observation of Figs. 1(a) and 1(b) reveals that the curves deviate from straight lines at around 150 K, which is much higher than T_C^{mag}, indicating strong short-range FM spin interactions in $CrGeTe_3$ above T_C^{mag}. The effective magnetic moment μ_{eff} is determined to be around $4.22\mu_B$ (parallel to the ab plane) and $4.35\mu_B$ (parallel to the c axis), which are close to the theoretical value expected for Cr^{3+} of $3.87\mu_B$ [25]. The insets of Figs. 1(a) and 1(b) show the isothermal magnetization $M(H)$ at 5 K exhibiting a typical FM behavior with the saturation field H_S of about 5 kOe (parallel to the ab plane) and 2.5 kOe (parallel to the c axis). In addition, the $M(H)$ curves show almost no coercive force for $CrGeTe_3$.

Figure 1(c) shows the variation of the zero-field specific heat (SH) $C_p(T)$ with temperature. The sharp anomaly in $C_p(T)$ at 64.8 K corresponds to the Curie temperature T_C^{SH}. Since $CrGeTe_3$ is a semiconductor [25], the electronic contribution to the heat capacity is not considered. The C_{mag} can be calculated by the following equations [42]:

$$C_{mag}(T) = C_p(T) - NC_V^{Debye}(T) \quad (1)$$

and

$$C_V^{Debye}(T) = 9R\left(\frac{T}{\Theta_D}\right)^3 \int_0^{\Theta_D/T} \frac{x^4 e^x}{(e^x-1)^2} dx, \quad (2)$$

where R is the molar gas constant, Θ_D is the Debye temperature, and $N = 5$ is the number of atoms per formula unit. The sum of Debye functions accounts for the lattice contribution to the specific heat. We can extract the magnetic contribution $C_{mag}(T)$ from the measured specific heat of $CrGeTe_3$. The fitted $C_p(T)$ for $CrGeTe_3$ by Eqs. (1) and (2)

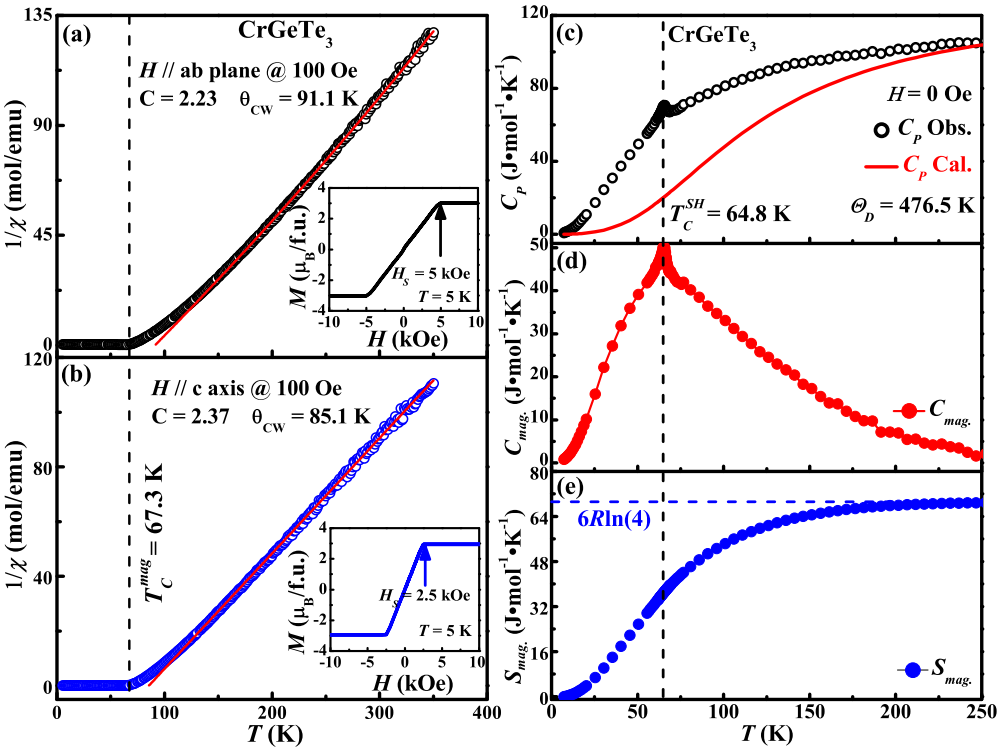

FIG. 1. (a) and (b) Temperature-dependent inverse susceptibility $1/\chi(T)$ of $CrGeTe_3$ under field cooled cooling with an applied magnetic field H of 100 Oe, parallel to the ab plane and c axis, respectively. The red solid lines are the fitted results according to the Curie-Weiss law. The insets show the isothermal magnetization curves $M(H)$ at 5 K. (c) Specific heat C_p as a function of T for $CrGeTe_3$ and the fitted $C_V^{Debye}(T)$ using Eqs. (1) and (2); temperature-dependent magnetic (d) specific heat $C_{mag}(T)$ and (e) entropy $S_{mag}(T \to \infty)$. The blue dashed line refers to $S_{mag}(T)$ calculated with the magnetic moment S of Cr^{3+} being 3/2.

over the temperature range from about 7 to 250 K is shown by the red curve in Fig. 1(c) using the Debye temperature $\Theta_D = 476.5$ K. We observe a sharp peak at T_C^{SH} of 64.8 K and there are strong dynamic short-range FM spin interactions above T_C^{SH} [see Fig. 1(d)]. The magnetic entropy $S_{mag}(T)$ is calculated by

$$S_{mag}(T) = \int_0^T \frac{C_{mag}(T)}{T} dT. \quad (3)$$

Figure 1(e) shows the temperature dependence of $S_{mag}(T)$. The entropy of $CrGeTe_3$ per mole with completely disordered spins S is

$$S_{mag}(T \to \infty) = 6R \ln(2S + 1). \quad (4)$$

Using $S = 3/2$ for Cr^{3+}, we obtain $S_{mag}(T \to \infty)$ of 69.2 J/(mol K). However, we observe the S_{mag} is 64.7 J/(mol K) at 150 K in Fig. 1(e), which is smaller than $S_{mag}(T \to \infty)$. Note that there is an error of about 10% [43] in our measurement due to the fitting of the optical phonon contributions at high temperatures. In spite of this small error, our result indicates the strong short-range FM spin interactions above T_C^{SH}.

As mentioned above, with the X atom radius increaseing, the $CrXTe_3$ compounds present the smaller van der Waals gap and the larger cleavage energy [7,25,28,31], which may induce a 3D magnetic phase transition. For the purpose of confirmation, we performed a detailed characterization of the critical phenomena using the initial isothermal $M(H)$ curves around T_C for the $CrGeTe_3$, which are shown in Fig. 2(a). In the mean-field theory (see the Supplemental Material [36]), the critical exponents and critical temperature can be determined from the Arrott plot with β of 0.5 and γ of 1.0 [44,45]. According to this method, the M^2 versus H/M [shown in Fig. 2(b)] should be a series of parallel straight lines in the higher field range around T_C and the line at $T = T_C$ should pass through the origin. Note that the lower-field data mainly represent the arrangement of magnetic domains, which should be excluded from the fitting process [46]. However, all the curves in Fig. 2(b) show nonlinear behaviors having downward curvature even at high fields, which indicates a non-mean-field-like behavior. Moreover, the positive slope reveals a second-order phase transition according to the criterion proposed by Banerjee [47]. As such, a modified Arrott plot should be employed to obtain the critical exponents.

To determine an accurate model, we obtain a modified Arrott plot following Eq. (S5) for single-crystalline $CrGeTe_3$ at different temperatures. Three groups of possible exponents belonging to the 3D Heisenberg model ($\beta = 0.365$, $\gamma = 1.386$), 3D-Ising model ($\beta = 0.325$, $\gamma = 1.24$), and tricritical mean-field model ($\beta = 0.25$, $\gamma = 1.0$) exhibit nearly straight lines in the high-field region [48,49]. We calculate their normalized slopes (NS) defined as $NS = S(T)/S(T_C^{mag} = 67.3\ K)$. By comparing the NS with the ideal value of unity, one can identify the most suitable model [48,49]. Figure 2(c) shows the plots of NS versus T employing the three different models, revealing that the tricritical mean-field model is the most appropriate to describe the critical behavior of $CrGeTe_3$.

By proper selections of β and γ, one can clearly show the isotherms are a set of parallel straight lines at high fields as

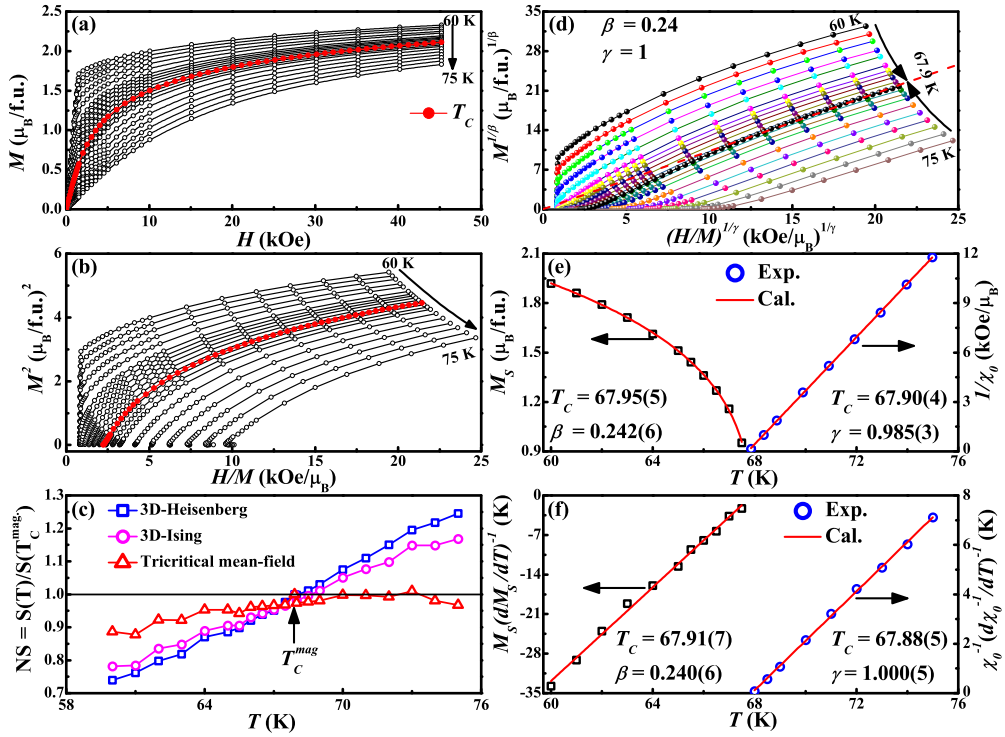

FIG. 2. (a) Initial magnetization of $CrGeTe_3$ around T_C. (b) Arrott plots of M^2 versus H/M [the $M(H)$ curves are measured at temperature intervals of 1 and 0.5 K approaching T_C]. (c) Normalized slopes as a function of temperature. (d) Modified Arrott plot [$M^{1/\beta}$ versus $(H/M)^{1/\gamma}$] of isotherms with $\beta = 0.24$ and $\gamma = 1$ for $CrGeTe_3$. The red dashed line is the linear fit of isotherm at 67.9 K. (e) Temperature dependence of M_S and χ_0^{-1}. The T_C and critical exponents are obtained from the fitting of Eqs. (S1) and (S2). (f) The Kouvel-Fisher plot. The T_C and critical exponents are obtained from the linear fit.

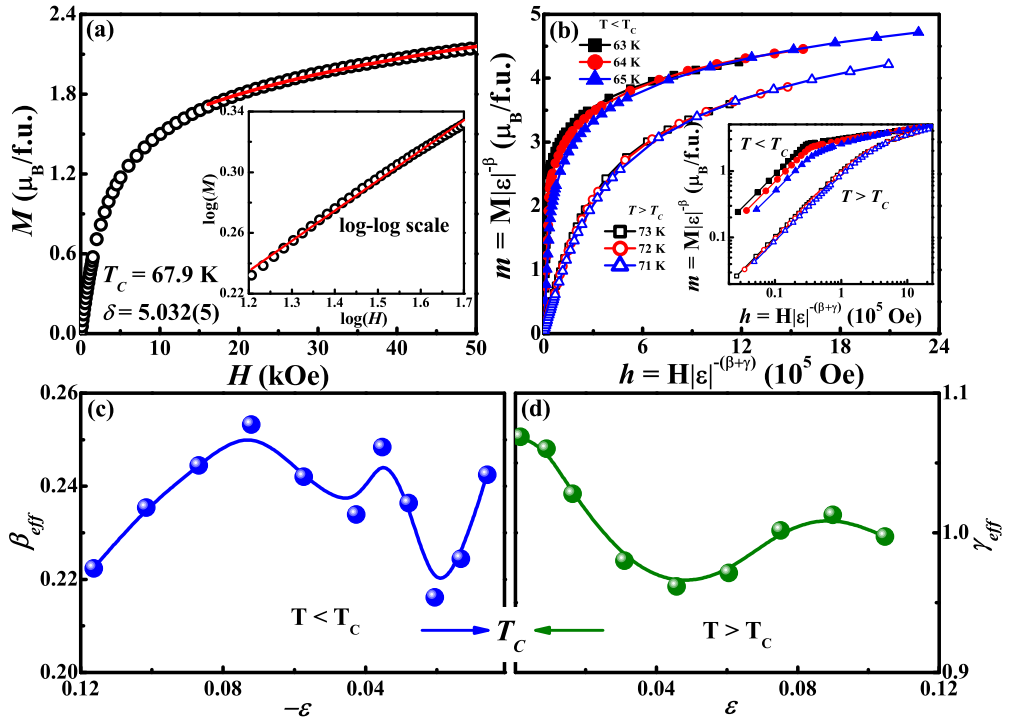

FIG. 3. (a) Isothermal $M(H)$ at T_C. The inset shows the alternative plot on a log-log scale and the straight line is the linear fit following Eq. (S3). (b) Renormalized magnetization m versus renormalized field h at several typical temperatures around the T_C. The inset shows an alternative plot on a log-log scale; the effective exponents (c) below T_C and (d) above T_C as a function of the reduced temperature ε.

displayed in Fig. 2(d). The linear extrapolation from the high-field region gives the spontaneous magnetization $M_S(T,0)$ and the initial inverse susceptibility $\chi_0^{-1}(T,0)$ [see Fig. 2(e)] corresponding to the intercepts on the $M^{1/\beta}$ and $(H/M)^{1/\gamma}$ axes, respectively. By fitting the data of $M_S(T,0)$ to Eqs. (S1) and (S2), one obtains two new values of $\beta = 0.242 \pm 0.006$ with $T_C = 67.95 \pm 0.01$ and $\gamma = 0.985 \pm 0.009$ with $T_C = 67.90 \pm 0.09$. These results are again very close to the critical exponents of the tricritical mean-field model. In addition, these critical exponents and T_C can be obtained more accurately from the Kouvel-Fisher (KF) method [50]. Hence, one can find that the temperature dependence of $M_S(dM_S/dT)^{-1}$ and $\chi_0^{-1}(d\chi_0^{-1}/dT)^{-1}$ should be straight lines with slopes $1/\beta$ and $1/\gamma$, respectively. As seen in Fig. 2(f), the linear fit yields the β of 0.240 ± 0.006 with T_C of 67.91 ± 0.07 and γ of 1.000 ± 0.005 with T_C of 67.88 ± 0.05, respectively. Remarkably, the obtained values of the critical exponents and T_C using the KF method are in excellent agreement with those using the modified Arrott plot based on the tricritical mean-field model. This suggests that the estimated values are self-consistent and unambiguous.

To further validate the above critical exponents β and γ, we study the relation among these exponents. According to Eq. (S3), δ can be directly estimated from the critical isotherm at T_C. Figure 3(a) shows the isothermal magnetization $M(H)$ at $T_C = 67.9$ K. The inset of the same plot has been demonstrated on a log-log scale. The solid straight line with a slope $1/\delta$ is the fitted result using Eq. (S3). From the linear fit we obtained the third critical exponent δ of 5.032 ± 0.005. Moreover, the exponent δ can be calculated by the Widom scaling relation [51,52]

$$\delta = 1 + \gamma/\beta. \tag{5}$$

Based on the β and γ values calculated in Figs. 2(e) and 2(f), Eq. (5) yields δ of 5.070 ± 0.006 and 5.167 ± 0.006, respectively. We emphasize that these values are very close to the results from the experimental critical isothermal analysis. Therefore, the critical exponents obtained in this study basically obey the Widom scaling relation, showing that the obtained β, γ, and δ are reliable.

Finally, these critical exponents should follow the scaling equation [Eq. (S6)] in the critical region. The scaling equation indicates that m versus h forms two universal curves for $T > T_C$ and $T < T_C$, respectively. Based on Eq. (S7), the

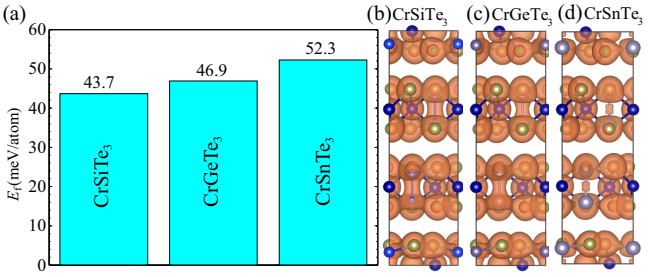

FIG. 4. (a) Formation energy of single-layer CrXTe$_3$. The formation energy of single-layer CrSiTe$_3$ is adopted from Ref. [55]. (b), (c), and (d) Charge density of bulk CrXTe$_3$ with an isosurface value of 0.05 e/r_{Bohr}^3.

TABLE I. Critical exponents of $CrGeTe_3$ with various theoretical models, $CrSiTe_3$, and other related materials with the tricritical mean-field model [SC, single crystal; PC, polycrystalline; cal, calculated from Eq. (5)].

Composition	Reference	T_C (K)	Technique	β	γ	δ
$CrGeTe_3^{SC}$	This work	67.9	Modified Arrott plot	0.242 ± 0.006	0.985 ± 0.003	5.070 ± 0.006^{cal}
			Kouvel-Fisher method	0.240 ± 0.006	1.000 ± 0.005	5.167 ± 0.005^{cal}
			Critical isotherm			5.032 ± 0.005
Tricritical mean-field	[47]		Theory	0.25	1	5
Mean-field	[44,45]		Theory	0.5	1	3
3D-Heisenberg theory	[44,45]		Theory	0.365	1.386	4.8
3D-Ising	[44,45]		Theory	0.325	1.24	4.82
$CrSiTe_3^{SC}$	[34]	31	Modified Arrott plot	0.170 ± 0.008	1.532 ± 0.001	10.012 ± 0.047^{cal}
$MnSi^{SC}$	[48]	30.5	Modified Arrott plot	0.242 ± 0.006	0.915 ± 0.003	4.734 ± 0.006
$La_{0.1}Nd_{0.6}Sr_{0.3}MnO_3^{PC}$	[49]	249.3	Modified Arrott plot	0.257 ± 0.005	1.12 ± 0.03	5.17 ± 0.02
$La_{0.9}Te_{0.1}MnO_3^{PC}$	[53]	239.5	Modified Arrott plot	0.201 ± 0.003	1.27 ± 0.04	7.14 ± 0.04
$La_{0.6}Ca_{0.4}MnO_3^{PC}$	[54]	265.5	Modified Arrott plot	0.25 ± 0.03	1.03 ± 0.05	5.0 ± 0.8

isothermal magnetization around the critical temperatures for $CrGeTe_3$ has been plotted in Fig. 3(b). All experimental data in the higher-field region collapse into two universal curves, in agreement with the scaling theory. The inset of Fig. 3(b) shows the corresponding log-log plot. Similarly, all the points collapse into two different curves in the higher-field region. This result shows again that the obtained results of the critical exponents and T_C are valid.

To further examine the convergence of the critical exponents, the effective exponents β_{eff} and γ_{eff} can be obtained by Eqs. (S8) and (S9) for $CrGeTe_3$. As shown in Figs. 3(c) and 3(d), both β_{eff} and γ_{eff} show a nonmonotonic variation with ε [see Eq. (S4)]. The lowest ε (ε_{min}) are 5.89×10^{-3} and 1.47×10^{-3} for β_{eff} and γ_{eff}, respectively. We obtain the effective exponents β_{eff} of 0.242 and γ_{eff} of 1.069, indicating that both β_{eff} and γ_{eff} are converged when the temperature approaches T_C.

The experimental critical exponents of $CrGeTe_3$, as well as the theoretical values of $CrSiTe_3$, MnSi, and some other manganites based on various models are summarized in Table I. It is seen that the critical exponents for MnSi and doped manganites are consistent with those of tricritical mean-field theory [48,49,53,54]. These compounds have the same characteristics, i.e., a tricritical point separating the first-order from the second-order ferromagnetic phase transitions. This phenomenon shows that the element substitution [49,54], hole or electric doping [53], and external magnetic field [48] can induce the tricritical behavior. However, $CrGeTe_3$ presents a second-order ferromagnetic phase transition [7,25–28] and our results indicate that the critical behavior of $CrGeTe_3$ is close to the theoretical value of the tricritical mean-field model. Comparing with $CrSiTe_3$, showing characteristics of the 2D-Ising model [7,34,35], the smaller van der Waals gap and the larger planar nearest-neighbor Cr-Cr distance of $CrGeTe_3$ enhances the Curie temperature from 32 K for the $CrSiTe_3$ to 61 K for the $CrGeTe_3$ [7,25–28]. In addition, the neutron scattering and isothermal magnetization experiments yield a critical exponent β of around 0.151 or 0.17 for $CrSiTe_3$ [7,34,35], which is close to the value expected for a 2D transition ($\beta_{2D}^{Ising} = 0.125$) and well below the value expected for a 3D transition ($\beta_{2D}^{Ising} = 0.326$). Our results yield a critical exponent β of 0.24 for $CrGeTe_3$ that is close to the critical exponent of the tricritical mean-field model. Hence, the increase of the X atom radius, facilitating superexchange coupling between the Cr atoms via the Te atoms and leading to the smaller van der Waals gap in the $CrXTe_3$ system [7,25–28], could induce a tricritical magnetic phase transition in the $CrGeTe_3$ single crystal.

Although single-crystalline $CrSnTe_3$ has not yet been synthesized, we speculate that the magnetism of $CrSnTe_3$ should be closer to the 3D-Ising model. To support this assumption, we perform DFT calculations with the same calculation parameters that were used in Ref. [55]. Figure 4(a) shows the calculated formation energy E_f, which is defined as the energy cost of extracting a sheet of single-layer $CrXTe_3$ from their bulk counterparts. As can be seen, E_f increases as the species vary from Si to Ge. This is consistent with the larger theoretical cleavage energy of single-layer $CrGeTe_3$ than that of $CrSiTe_3$, which indicates that the layers are coupled more strongly in $CrGeTe_3$ [31]. The formation energy of $CrSnTe_3$ is even higher than the other two compounds, revealing that it presents the strongest interlayer coupling, which leads to its 3D characteristics. Figures 4(b), 4(c) and 4(d) illustrate the charge density of the three compounds. Consistent with the trend of the E_f results, the electron density around the Sn-Sn pair is the least among the three materials. Namely, more electrons in $CrSnTe_3$ participate in the interlayer coupling.

IV. CONCLUSIONS

In conclusion, we have performed a comprehensive experimental study on the critical properties of single-crystalline $CrGeTe_3$ using isothermal magnetization around the Curie temperature T_C. Based on various experimental techniques including the modified Arrott plot, KF method, and critical isotherm analysis, we obtained the critical exponents β, γ, and δ of 0.240 ± 0.006, 1.000 ± 0.005, and 5.070 ± 0.006, respectively, at the Curie temperature of 67.9 K. These numerical results are similar to the theoretical values in the tricritical mean-field model, which is therefore capable of describing the critical magnetic behavior of 2D $CrGeTe_3$. DFT calculations show that the formation energy of $CrGeTe_3$ lies between those of $CrSiTe_3$ and $CrSnTe_3$, which is in line with a crossover of the magnetic phase transition from 2D to 3D.

Overall, our findings provide a fundamental understanding of the anomalous PM-FM transition in a novel 2D ferromagnetic semiconductor.

ACKNOWLEDGMENTS

This work was supported by the National Key Research and Development Program under Contracts No. 2016YFA0300404 and No. 2016YFA0401003, the Joint Funds of the National Natural Science Foundation of China and the Chinese Academy of Sciences' Large-Scale Scientific Facility under Contracts No. U1432139 and No. U1532153, the National Natural Science Foundation of China under Contract No. 11674326, Key Research Program of Frontier Sciences, CAS (QYZDB-SSW-SLH015), and the Nature Science Foundation of Anhui Province under Contract No. 1508085ME103. J.Z. is supported by the Nature Science Foundation of China (Grant No. 51602079) and the Fundamental Research Funds for the Central Universities of China (Grant No. 372 AUGA5710013115). This research also used computational resources of the National Supercomputing Center of China in Shenzhen (Shenzhen Cloud Computing Center).

[1] K. S. Novoselov, A. K. Geim, S. V. Morozov, D. Jiang, Y. Zhang, S. V. Dubonos, I. V. Grigorieva, and A. A. Firsov, Science **306**, 666 (2004).
[2] K. S. Novoselov, A. K. Geim, S. Morozov, D. Jiang, M. Katsnelson, I. Grigorieva, S. Dubonos, and A. Firsov, Nature (London) **438**, 197 (2005).
[3] Y. Zhang, Y.-W. Tan, H. L. Stormer, and P. Kim, Nature (London) **438**, 201 (2005).
[4] A. K. Geim and K. S. Novoselov, Nat. Mater. **6**, 183 (2007).
[5] A. H. Castro Neto, F. Guinea, N. M. R. Peres, K. S. Novoselov, and A. K. Geim, Rev. Mod. Phys. **81**, 109 (2009).
[6] N. Zibouche, A. Kuc, J. Musfeldt, and T. Heine, Ann. Phys. (N.Y.) **526**, 395 (2014).
[7] T. J. Williams, A. A. Aczel, M. D. Lumsden, S. E. Nagler, M. B. Stone, J.-Q. Yan, and D. Mandrus, Phys. Rev. B **92**, 144404 (2015).
[8] I. Žutić, J. Fabian, and S. Das Sarma, Rev. Mod. Phys. **76**, 323 (2004).
[9] A. MacDonald, P. Schiffer, and N. Samarth, Nat. Mater. **4**, 195 (2005).
[10] T. Dietl, Nat. Mater. **9**, 965 (2010).
[11] Z. Deng, C. Jin, Q. Liu, X. Wang, J. Zhu, S. Feng, L. Chen, R. Yu, C. Arguello, T. Goko *et al.*, Nat. Commun. **2**, 422 (2011).
[12] Z. Y. Zhu, Y. C. Cheng, and U. Schwingenschlögl, Phys. Rev. B **84**, 153402 (2011).
[13] D. Xiao, G.-B. Liu, W. Feng, X. Xu, and W. Yao, Phys. Rev. Lett. **108**, 196802 (2012).
[14] W. Feng, Y. Yao, W. Zhu, J. Zhou, W. Yao, and D. Xiao, Phys. Rev. B **86**, 165108 (2012).
[15] W.-Y. Shan, H.-Z. Lu, and D. Xiao, Phys. Rev. B **88**, 125301 (2013).
[16] X. Xu, W. Yao, D. Xiao, and T. F. Heinz, Nat. Phys. **10**, 343 (2014).
[17] W. Han, R. K. Kawakami, M. Gmitra, and J. Fabian, Nat. Nanotechnol. **9**, 794 (2014).
[18] H. Ohno, D. Chiba, F. Matsukura, T. Omiya, E. Abe, T. Dietl, Y. Ohno, and K. Ohtani, Nature (London) **408**, 944 (2000).
[19] C.-Z. Chang, J. Zhang, X. Feng, J. Shen, Z. Zhang, M. Guo, K. Li, Y. Ou, P. Wei, L.-L. Wang *et al.*, Science **340**, 167 (2013).
[20] X. Kou, S.-T. Guo, Y. Fan, L. Pan, M. Lang, Y. Jiang, Q. Shao, T. Nie, K. Murata, J. Tang, Y. Wang, L. He, T.-K. Lee, W.-L. Lee, and K. L. Wang, Phys. Rev. Lett. **113**, 137201 (2014).
[21] Z. Wang, C. Tang, R. Sachs, Y. Barlas, and J. Shi, Phys. Rev. Lett. **114**, 016603 (2015).
[22] H. González-Herrero, J. M. Gómez-Rodríguez, P. Mallet, M. Moaied, J. J. Palacios, C. Salgado, M. M. Ugeda, J.-Y. Veuillen, F. Yndurain, and I. Brihuega, Science **352**, 437 (2016).
[23] C. Gong, L. Li, Z. Li, H. Ji, A. Stern, Y. Xia, T. Cao, W. Bao, C. Wang, Y. Wang *et al.*, Nature **546**, 265 (2017).
[24] N. Sivadas, M. W. Daniels, R. H. Swendsen, S. Okamoto, and D. Xiao, Phys. Rev. B **91**, 235425 (2015).
[25] V. Carteaux, D. Brunet, G. Ouvrard, and G. Andre, J. Phys.: Condens. Matter **7**, 69 (1995).
[26] H. Ji, R. Stokes, L. Alegria, E. Blomberg, M. Tanatar, A. Reijnders, L. Schoop, T. Liang, R. Prozorov, K. Burch *et al.*, J. Appl. Phys. **114**, 114907 (2013).
[27] Y. Tian, M. J. Gray, H. Ji, R. Cava, and K. S. Burch, 2D Materials **3**, 025035 (2016).
[28] H. L. Zhuang, Y. Xie, P. R. C. Kent, and P. Ganesh, Phys. Rev. B **92**, 035407 (2015).
[29] B. Siberchicot, S. Jobic, V. Carteaux, P. Gressier, and G. Ouvrard, J. Phys. Chem. **100**, 5863 (1996).
[30] S. Lebègue, T. Björkman, M. Klintenberg, R. M. Nieminen, and O. Eriksson, Phys. Rev. X **3**, 031002 (2013).
[31] X. Li and J. Yang, J. Mater. Chem. C **2**, 7071 (2014).
[32] J. Zhang, B. Zhao, Y. Yao, and Z. Yang, Phys. Rev. B **92**, 165418 (2015).
[33] J. Liu, S. Y. Park, K. F. Garrity, and D. Vanderbilt, Phys. Rev. Lett. **117**, 257201 (2016).
[34] B. Liu, Y. Zou, L. Zhang, S. Zhou, Z. Wang, W. Wang, Z. Qu, and Y. Zhang, Sci. Rep. **6**, 33873 (2016).
[35] V. Carteaux, F. Moussa, and M. Spiesser, Europhys. Lett. **29**, 251 (1995).
[36] See Supplemental Material at http://link.aps.org/supplemental/10.1103/PhysRevB.95.245212 for XRD patterns and the scaling analysis, which includes Refs. [25,26,48,56–61].
[37] G. Kresse and J. Furthmüller, Phys. Rev. B **54**, 11169 (1996).
[38] D. M. Ceperley and B. J. Alder, Phys. Rev. Lett. **45**, 566 (1980).
[39] J. P. Perdew and A. Zunger, Phys. Rev. B **23**, 5048 (1981).
[40] P. E. Blöchl, Phys. Rev. B **50**, 17953 (1994).
[41] G. Kresse and D. Joubert, Phys. Rev. B **59**, 1758 (1999).
[42] C. Kittel, *Introduction to Solid State Physics* (Wiley, New York, 2004).
[43] N. Tristan, J. Hemberger, A. Krimmel, H.-A. Krug von Nidda, V. Tsurkan, and A. Loidl, Phys. Rev. B **72**, 174404 (2005).
[44] A. Arrott, Phys. Rev. **108**, 1394 (1957).
[45] S. Kaul, J. Magn. Magn. Mater. **53**, 5 (1985).

[46] N. Khan, P. Mandal, K. Mydeen, and D. Prabhakaran, Phys. Rev. B **85**, 214419 (2012).
[47] B. Banerjee, Phys. Lett. **12**, 16 (1964).
[48] L. Zhang, D. Menzel, C. Jin, H. Du, M. Ge, C. Zhang, L. Pi, M. Tian, and Y. Zhang, Phys. Rev. B **91**, 024403 (2015).
[49] J. Fan, L. Ling, B. Hong, L. Zhang, L. Pi, and Y. Zhang, Phys. Rev. B **81**, 144426 (2010).
[50] J. S. Kouvel and M. E. Fisher, Phys. Rev. **136**, A1626 (1964).
[51] B. Widom, J. Chem. Phys. **43**, 3898 (1965).
[52] B. Widom, J. Chem. Phys. **41**, 1633 (1964).
[53] J. Yang, Y. P. Lee, and Y. Li, Phys. Rev. B **76**, 054442 (2007).
[54] D. Kim, B. Revaz, B. L. Zink, F. Hellman, J. J. Rhyne, and J. F. Mitchell, Phys. Rev. Lett. **89**, 227202 (2002).
[55] M.-W. Lin, H. L. Zhuang, J. Yan, T. Z. Ward, A. A. Puretzky, C. M. Rouleau, Z. Gai, L. Liang, V. Meunier, B. G. Sumpter *et al.*, J. Mater. Chem. C **4**, 315 (2016).
[56] H. E. Stanley, *Introduction to Phase Transitions and Critical Phenomena* (Oxford University Press, New York, 1971).
[57] A. K. Pramanik and A. Banerjee, Phys. Rev. B **79**, 214426 (2009).
[58] M. E. Fisher, Rep. Prog. Phys. **30**, 615 (1967).
[59] A. Arrott and J. E. Noakes, Phys. Rev. Lett. **19**, 786 (1967).
[60] N. Khan, A. Midya, K. Mydeen, P. Mandal, A. Loidl, and D. Prabhakaran, Phys. Rev. B **82**, 064422 (2010).
[61] A. Perumal, V. Srinivas, V. V. Rao, and R. A. Dunlap, Phys. Rev. Lett. **91**, 137202 (2003).